SAND2019-11472R

Sandia National Laboratories

Operated for the U.S. Department of Energy
by National Technology and Engineering Solutions
of Sandia, LLC.

Albuquerque, New Mexico 87185
Livermore, California 94551

date: September 17, 2019

to: Distribution

from: B. T. Lester (1554), K. Long (1554)

subject: Numerical Integration of Viscoelastic Models

1 Introduction

Accurate modeling of viscoelasticity remains an important consideration for a variety of materials (*e.g.* polymers [1] and inorganic glasses [2, 3]). As such, over the previous decades a substantial body of work has been dedicated to developing appropriate constitutive models for viscoelasticity ranging from initial considerations of linear thermoviscoelasticity [4, 5] to more complex non-linear formulations incorporating fictive temperatures [2] or potential energy clocks [1, 6] including the use of both internal state variable (ISV) [7] and hereditary integral [1] representations.

Nonetheless, relatively limited (in comparison to plasticity) attention has been paid to the numerical integration of such schemes. In terms of integral based formulations, Taylor *et al.* [8] first considered the problem of the integration of a linear viscoelasticity model. That work focused on the integration of the hereditary integrals and demonstrated improved performance of the new scheme with a custom finite element code over an existing finite difference reference. Chambers and Becker [9], using a free volume based shift factor, also considered the integration of the hereditary integrals and the impact on the problem of a pressurized thick-walled cylinder and developed an adaptive scheme to bound the error. Chambers [10] later developed three-point Gauss and composite integration schemes for the hereditary integrals and noted improved accuracy. With respect to ISV-based schemes, formulations for the non-linear Schapery model [11, 12] have been proposed. However, in those efforts greater attention was paid to convergence of the non-linear solution scheme than impact of numerical integration. Various authors (*e.g.* Holzapfel [13] and Simo and Hughes [14]) have also studied the use of convolution integrals with differential forms of ISVs for temperature-independent formulations.

Regardless, while the "potential energy clock" (PEC) [1] and "simplified potential energy clock" (SPEC) [6] models have been used to study a variety of non-linear responses (*e.g.* [15, 16, 3]), limited attention has been paid to the numerical performance. As will be discussed later, the "clock" at the center of the formulations includes temperature and complex history dependence making the numerical integration of such a model even more challenging. Thus, in the current work an initial effort towards characterizing the numerical integration of the constitutive model through simplified problems is performed. To that end, in Section 2 the theory of the model is briefly presented while the numerical integration is discussed in Section 3. Results of various studies characterizing the numerical behavior and performance are then given in Section 4. Finally, some concluding remarks and thoughts for follow on works are provided in Section 5.

2 Theory

The SPEC model [6] of interest here is, as the name implies, a simplified version of the the PEC model of Caruthers *et al.* [1]. While details of the formulations are left to those works, the model is briefly reviewed here to enable subsequent discussions. To this end the Cauchy stress[1], σ_{ij}, may be written,

$$\begin{aligned}\sigma_{ij} &= \frac{\rho}{\rho_0}\left[K_d\left(T\right)\int_0^t f_v\left(t^*-s^*\right)\frac{dI_1}{ds}\mathrm{d}s - L_d\left(T\right)\int_0^t f_v\left(t^*-s^*\right)\frac{dT}{ds}\mathrm{d}s\right]\delta_{ij} \\ &\quad +2\frac{\rho}{\rho_0}G_d\left(T\right)\int_0^t f_s\left(t^*-s^*\right)d'_{ij}\mathrm{d}s + \frac{\rho}{\rho_0}\left[K_\infty\left(T\right)I_1 - L_\infty\left(T\right)\left(T-T_{\mathrm{ref}}\right)\right]\delta_{ij} \\ &\quad +2\frac{\rho}{\rho_0}G_\infty\left(T\right)\varepsilon'_{ij},\end{aligned} \tag{1}$$

in which ρ, ρ_0, β and T are the current density, reference density, volumetric coefficient of thermal expansion, and temperature while K, G, and L and the bulk, shear, and thermal ($L = K\beta$) moduli with the subscript "d" denoting the difference between glassy (subscript "g") and equilibrium ("∞") phase such that $x_d = x_g - x_\infty$. Furthermore, d_{ij} and ε_{ij} are the unrotated rate of deformation and strain[2] and the "$\prime$" denotes the deviatoric component of a tensor such that $x'_{ij} = x_{ij} - (1/3)x_{kk}\delta_{ij}$ while I_1 is the first invariant of the strain tensor ($I_1 = \varepsilon_{kk}$).

[1]The current written form is an approximation to the Cauchy stress given by Adolf *et al.* [6] assuming small rotations. In both the original PEC model and subsequent SPEC formulation substantial attention is paid the choice of finite deformation strain and stress measure and the impact on the formulation. For clarity of the current presentation, such details are being bypassed by assuming small rotations (such that $R_{ij} = \delta_{ij}$) and referring the reader to the work of Caruthers *et al.* [1] and Adolf *et al.* [6] for detailed discussion to that end. Further, while for presentation purposes small rotations are assumed, the model implementation was not changed and as such makes no such assumption/limitation.

[2]Specifically, in this case the strain measure is the integrated unrotated rate of deformation.

The integrals in Eqn. 1 are hereditary integrals capturing the history of the thermomechanical state. Specifically, f_v and f_s are the bulk and shear relaxation spectra, respectively, in this case represented by different Prony series. The "$*$" denotes "material" time which represents the time frame in which the viscoelastic processes are occurring. It may be related to the current "physical" or "laboratory" time, t, via a single shift factor, a, such that,

$$t^* - s^* = \int_s^t \frac{\mathrm{d}x}{a\left(x\right)}. \tag{2}$$

In the PEC and SPEC models, the shift factor is determined via the current value of a material clock, N. For the SPEC formalism, these terms may be related via,

$$\log a = -\frac{C_1 N}{C_2'' + N}, \tag{3}$$

with,

$$\begin{aligned} N \;=\; & \left[\left(T - T_{\mathrm{ref}}\right) - \int_0^t f_v\left(t^* - s^*\right)\frac{dT}{ds}\mathrm{d}s\right] + C_3\left[I_1 - \int_0^t f_v\left(t^* - s^*\right)\frac{dI_1}{ds}\mathrm{d}s\right] \\ & + C_4 \int_0^t \int_0^t f_s\left(t^* - s^*, t^* - u^*\right) d'_{ij}\left(s\right) d'_{ij}\left(u\right) \mathrm{d}s\mathrm{d}u, \end{aligned} \tag{4}$$

where C_1 and C_2 are the WLF [17] constants and the remaining constants (denoted by C) may be approximated as,

$$\begin{aligned} C_2'' \;=\; & C_2\left[1 + C_3\beta_\infty^{\mathrm{ref}}\right] \cong C_2\left[1 + \frac{T_{\mathrm{ref}} L_d^{\mathrm{ref}} \beta_\infty^{\mathrm{ref}}}{\rho_0 C_{\mathrm{V}d}^{\mathrm{ref}}}\right], \\ & C_3 \approx \frac{T_{\mathrm{ref}} L_d^{\mathrm{ref}}}{\rho_0 C_{\mathrm{V}d}^{\mathrm{ref}}}, \qquad C_4 \approx -\frac{G_d^{\mathrm{ref}}}{\rho_0 C_{\mathrm{V}d}^{\mathrm{ref}}}, \end{aligned} \tag{5}$$

and a superscript "ref" denotes a temperature dependent quantity evaluated at $T = T_{ref}$ and C_{v} is the specific heat at constant volume.

3 Numerical Integration

For a displacement-based finite element program, in which the temperature history is known and a strain increment is prescribed, it may be observed from Eqn. 1 that updating the stress revolves around being able to appropriately evaluate the hereditary integrals. However, the relaxation spectra forming the core of these integrals are defined in terms of the

material time and, correspondingly, the clock. From Eqn. 4 it may be observed that the clock has substantial history dependence and is implicitly defined. As such, the clock is implicitly defined and a corresponding non-linear numerical solve is needed to perform the stress update. In this instance, a Newton-Raphson scheme is used to find the current value of the clock. Additionally, throughout all of these operations, the integrals needed to be continually reevaluated. Thus, two different numerical operations are needed to perform the stress integration (*i*) numerical integration of the hereditary integrals and (*ii*) determination of the material clock. Both will be briefly described here while additional details may be found in the LAMÉ manual [18].

3.1 Hereditary Integral Integration

First, the ability to accurately and efficiently evaluate the hereditary integrals is a well recognized problem for viscoelasticity (*e.g.* [8, 10]). To emphasize this point, Eqns. 1 and 4 may be recast,

$$\begin{aligned}\sigma_{ij} &= \frac{\rho}{\rho_0}\left[K_d\left(T\right)J_1 - L_d\left(T\right)J_3\right]\delta_{ij} \\ &\quad +2\frac{\rho}{\rho_0}G_d\left(T\right)H_{ij} + \frac{\rho}{\rho_0}\left[K_\infty\left(T\right)I_1 - L_\infty\left(T\right)\left(T-T_{\text{ref}}\right)\right]\delta_{ij} \\ &\quad +2\frac{\rho}{\rho_0}G_\infty\left(T\right)\varepsilon'_{ij}, \end{aligned} \tag{6}$$

$$\begin{aligned}N &= \left[\left(T-T_{\text{ref}}\right) - J_3\right] + C_3\left[I_1 - J_1\right] \\ &\quad +C_4 Q, \end{aligned} \tag{7}$$

where

$$J_1 = \int_0^t f_v\left(t^*-s^*\right)\frac{dI_1}{ds}\mathrm{d}s, \tag{8}$$

$$H_{ij} = \int_0^t f_s\left(t^*-s^*\right)d'_{ij}\mathrm{d}s, \tag{9}$$

$$J_3 = \int_0^t f_v\left(t^*-s^*\right)\frac{dT}{ds}\mathrm{d}s, \tag{10}$$

$$Q = \int_0^t\int_0^t f_s\left(t^*-s^*,t^*-u^*\right)d'_{ij}\left(s\right)d'_{ij}\left(u\right)\mathrm{d}s\mathrm{d}u. \tag{11}$$

If arbitrary functions are allowed to represent the relaxation spectra, each value of the integral would have to be stored leading to prohibitively expensive storage requirements for viscoelastic models. However, this problem has long been addressed by restricting the functional representations to specific classes of forms which can remove such a need. For the PEC and SPEC models (see [1, 6]), Prony series are used to this end such that,

$$f\left(t^*-s^*,t^*-u^*\right)=\sum_k w_k \exp\left(-\frac{t^*-s^*}{\tau_k}\right)\exp\left(-\frac{t^*-u^*}{\tau_k}\right). \tag{12}$$

Note the shorthand,

$$f\left(t^*-s^*\right)=f\left(t^*-s^*,0\right)=\sum_k w_k \exp\left(-\frac{t^*-s^*}{\tau_k}\right) \tag{13}$$

has been used. In the previous relations, k is the number of Prony terms in the series, τ_k is the k^{th} characteristic time and w_k is the corresponding weight. As prefactors may be found leading the integral, the spectra here are normalized such that $0 \leq f\left(x\right) \leq 1$ with $\sum_k w_k = 1$.

Written in this way, $J_1,\ H_{ij},\ J_3$, and Q contain the time history and are the terms that need to be numerically integrated. To that end, approaches to integrate J_3 shall be discussed and the underlying schemes may be easily extended to the other variables and therefore will not be presented for clarity. As a first step, it is noted that

$$J_3=\int_0^t \sum_{k=1}^{n_v} w_k^v \exp\left(-\frac{t^*-s^*}{\tau_k^v}\right)\frac{dT}{ds}\mathrm{d}s=\sum_{k=1}^{n_v} w_k^v \int_0^t \exp\left(-\frac{t^*-s^*}{\tau_k^v}\right)\frac{dT}{ds}\mathrm{d}s, \tag{14}$$

and by introducing,

$$J_3^k=\int_0^t \exp\left(-\frac{t^*-s^*}{\tau_k^v}\right)\frac{dT}{ds}\mathrm{d}s, \tag{15}$$

may be rewritten,

$$J_3=\sum_{k=1}^{n_v} w_k^v J_3^k, \tag{16}$$

in which n_v is the number of volumetric spectra Prony terms and a superscipt v denotes a corresponding volumetric quantity. As the weights (w_k^v) are constant,

$$\frac{dJ_3}{dt}=\sum_{k=1}^{n_v} w_k^v \frac{dJ_3^k}{dt}, \tag{17}$$

and by differentiating Eqn. 15 it can be shown that,

$$\frac{dJ_3^k}{dt} = \frac{dT}{dt} - \frac{1}{a\tau_k^v} J_3^k. \tag{18}$$

Thus, by considering Eqn. 16 it may be observed that J_3 may be found by updating each J_3^k via Eqn. 18. However, the derivative in Eqn. 18 is implicit in the current value of J_3^k necessitating a numerical approximation to be able to integrate the term appropriately. Multiple schemes may be used to perform such an operation. The approach that is currently used with the SPEC model is a variant of a midstep scheme [6, 18]. Specifically, consider a timestep $\Delta t = t_{n+1} - t_n$ where time t_n is a completely known state. Evaluating Eqn. 18 at the midstep $t_{n+1/2} = (1/2)\,(t_{n+1} + t_n)$ yields,

$$\frac{dJ_3^k}{dt}|_{t_{n+1/2}} = -\frac{1}{a_{n+1/2}\tau_k^v} \left(J_3^k\right)_{n+1/2} + \frac{T_{n+1} - T_n}{\Delta t}, \tag{19}$$

with subscripts $n,\ n+1/2$, and $n+1$ denoting values at $t_n,\ t_{n+1/2}$, and t_{n+1}, respectively. If the rate dJ_3^k/dt is approximated as constant over the timestep Δt such that,

$$\frac{dJ_3^k}{dt} \approx \frac{\left(J_3^k\right)_{n+1} - \left(J_3^k\right)_n}{\Delta t}, \tag{20}$$

the value at the midstep may be taken to be,

$$\left(J_3^k\right)_{n+1/2} \approx \frac{\left(J_3^k\right)_{n+1} + \left(J_3^k\right)_n}{2}. \tag{21}$$

Solving Eqns. 19–21 for the updated value produces,

$$\left(J_3^k\right)_{n+1} = \left(\frac{2a_{n+1/2}\tau_k^v - \Delta t}{2a_{n+1/2}\tau_k^v + \Delta t}\right) \left(J_3^k\right)_n + \left(\frac{2a_{n+1/2}\tau_k^v}{2a_{n+1/2}\tau_k^v + \Delta t}\right) (T_{n+1} - T_n)\,. \tag{22}$$

Alternative approaches may be derived from consideration of a typical, general integration scheme with,

$$\left(J_3^k\right)_{n+1} = \left(J_3^k\right)_n + (1-\beta)\,\Delta t \frac{dJ_3^k}{dt}|_{t_n} + \beta \Delta t \frac{dJ_3^k}{dt}|_{t_{n+1}}, \tag{23}$$

and $\beta = [0, 1]$ being the integration parameter such that $\beta = 0$ results in a foward Euler, explicit integration scheme, $\beta = 1/2$ is a midstep rule, and $\beta = 1$ is a backward Euler, implicit scheme. Such approaches are fairly standard (see *e.g.* [19]). To that end, if the fully implicit case of $\beta = 1$ is considered,

$$\left(J_3^k\right)^{n+1} = \left(\frac{a_{n+1}\tau_k^v}{a_{n+1}\tau_k^v + \Delta t}\right)\left(\left(J_3^k\right)^n + \Delta T\right), \tag{24}$$

where $\Delta T = T_{n+1} - T_n$. In what follows, the backward Euler approach of Eqn. 24 will be used as a comparison benchmark. The forward Euler scheme is not considered due to potential timestep size limitations associated with stability of such schemes and the $\beta = 0.5$ scheme is not considered as the existing method is already a midstep variant.

3.2 Material Clock Determination

Finding the current value of the material clock revolves around solving the non-linear equation posed by Eqn. 3 that depends on the complex history dependent clock, N, defined by Eqns. 4 and 7. For the current purposes a pure thermal loading shall be considered by setting $C_3 = C_4 = 0$ such that,

$$N = T - T_{\text{ref}} - J_3. \tag{25}$$

Extending the solution is straightforward in the case of $C_3 = C_4 \neq 0$. However, those cases require some tensorial derivatives that, while reasonably straighforward, may be cumbersome and as such are neglected for simplicity and clarity of presentation.

In residual form, the non-linear Eqn. 3 may be rewritten,

$$r^a = \log_{10} a + \frac{C_1 N}{C_2'' + N} = 0, \tag{26}$$

providing the equation to be solved for a. Introducing "m" to be a non-linear correction iteration, Eqn. 26 may be linearized such that,

$$r_{m+1}^a = r_m^a + \frac{1}{a \ln 10}\Delta a + \frac{C_1}{C_2'' + N}\frac{\partial N}{\partial a}\left(1 - \frac{N}{C_2'' + N}\right)\Delta a, \tag{27}$$

with Δa being the non-linear correction in a such that $a_{m+1} = a_m + \Delta a$. Noting that temperature is fixed over a correction iteration and independent of a,

$$\frac{\partial N}{\partial a} = -\frac{\partial J_3}{\partial a} = -\sum_{k=1}^{n_v} w_k^v \frac{\partial J_3^k}{\partial a}. \tag{28}$$

As J_3^k depends implicitly on a (see Eqn. 15) directly determining/evaluating the corresponding derivative can be complicated. However, Eqns. 22 and 24 provide expressions that may

be readily differentiated in terms of a_{n+1}[3]. Setting $r^a_{m+1} = 0$, Eqn. 27 may be solved for Δa as,

$$\Delta a = -\left[\frac{\left(C_2'' + N\right)^2 a \ln 10}{\left(C_2'' + N\right)^2 - a\left(\ln 10\right) C_1 C_2'' \frac{\partial J_3}{\partial a}}\right] r^a_m. \tag{29}$$

4 Results

To evaluate the numerical performance and convergence of the SPEC model, the parameterization of a representative inorganic glass (Schott 8061) given in a recent work by Chambers *et al.* [3] is used. This specific calibration is selected as it is a recent, complete set resulting from thorough characterization and validated against a variety of experiments. The non-zero model parameters (as provided by Chambers *et al.* [3]) are given in Table 1. Additionally, Table 2 presents the relaxation spectra used for this study. Note, in their work Chambers *et al.* only give the bulk spectra parameterized in terms of a stretched exponential. Here, the full spectra (in terms of weights and times) are presented for consistency and completeness. The following sections will present and discuss results from different representative loadings. Finite element simulations are performed with Sierra/SolidMechanics [20].

K_g	33 GPa	K_∞	6 GPa
$\mathrm{d}K_g/\mathrm{d}T$	-20.5 MPa/°C	$\mathrm{d}K_\infty/\mathrm{d}T$	-5.9 MPa/°C
β_g	27×10^{-6} °C^{-1}	β_∞	90×10^{-6} °C^{-1}
G_g	24.8 GPa	G_∞	248 kPa
$\mathrm{d}G_g/\mathrm{d}T$	-7.0 MPa/°C	$\mathrm{d}G_\infty/\mathrm{d}T$	0
C_1	17 (-)	C_2	350°C
T_{ref}	460°C		

Table 1: Non-zero SPEC model parameters provided by Chambers *et al.* [3].

4.1 No-load Cool

As a first consideration, the simple problem of a no-load cooling is considered. Specifically, the material is assumed to be initially at 510°C ($T_{\mathrm{ref}} + 50$) and cooled to a temperature of 150°C ($T_{\mathrm{ref}} - C_2 + 40$). Noting the implicit assumption in Eqn. 22 of a constant rate of change over a load step, a particular response of interest is a non-linear temperature profile. To this end, the expression,

$$T\left(t\right) = T_{\mathrm{high}} + \left(T_{\mathrm{low}} - T_{\mathrm{high}}\right)\left(\frac{t}{t_f}\right)^k \tag{30}$$

[3]Such an approach also has advantages in terms of consistency between the hereditary integral integration and linearization.

τ_k (s)	w_k^s	w_k^v
1×10^{-9}	0	4.42389×10^{-4}
1×10^{-8}	4.24345×10^{-3}	7.38956×10^{-4}
1×10^{-7}	6.63991×10^{-3}	1.53310×10^{-3}
1×10^{-6}	6.55255×10^{-3}	3.02200×10^{-3}
1×10^{-5}	1.41373×10^{-2}	6.04301×10^{-3}
1×10^{-4}	1.40109×10^{-2}	1.19125×10^{-2}
1×10^{-3}	2.01033×10^{-2}	2.36083×10^{-2}
1×10^{-2}	2.66430×10^{-2}	4.54541×10^{-2}
1×10^{-1}	4.31981×10^{-2}	8.68161×10^{-2}
1	5.98391×10^{-2}	1.51936×10^{-1}
1×10^{1}	1.46465×10^{-1}	2.43200×10^{-1}
1×10^{2}	1.62036×10^{-1}	2.51843×10^{-1}
1.9953×10^{2}	2.57094×10^{-1}	2.54964×10^{-2}
1×10^{3}	2.39037×10^{-1}	1.35599×10^{-1}
1×10^{4}	0	1.23552×10^{-2}

Table 2: Normalized relaxation spectra for use with the SPEC model parameterization provided by Chambers *et al.* [3].

is used for the temperature profile. The final time, t_f, is the total time it would take for a linear profile ($k = 1$) to cool at 5°C/min. The considered profiles are given in Fig. 1.

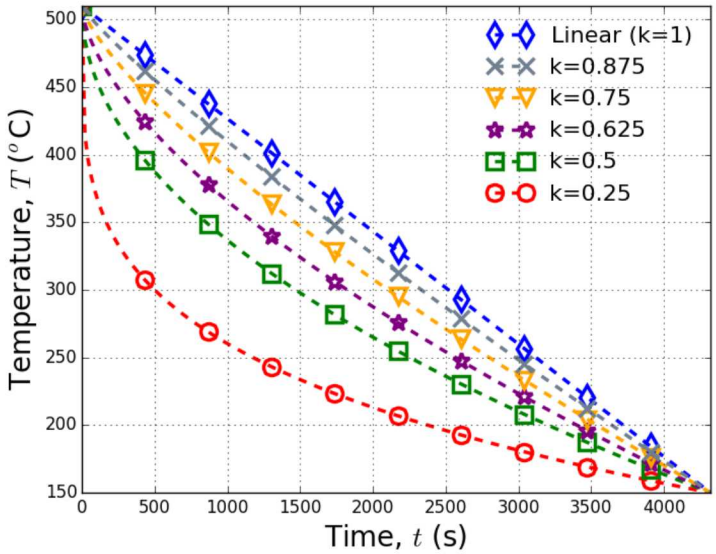

Figure 1: Temperature profiles considered for the no-load cooling simulations.

Results from finite element simulations with different values of k and various fixed, constant

timesteps are given in Fig. 2. Specifically, the relative error for the strain[4] (Fig. 2a), hereditary integral J_3 (Fig. 2c), and the log of the shift factor ($\log_{10} a$; Fig. 2c) are presented. The solution of simulations using a fixed timestep of $\Delta t = 0.5$s are assumed to be converged and taken as reference values for purposes of computing relative errors. Additionally, for smaller values of k larger timesteps did not converge. In those cases, the data is simply not reported.

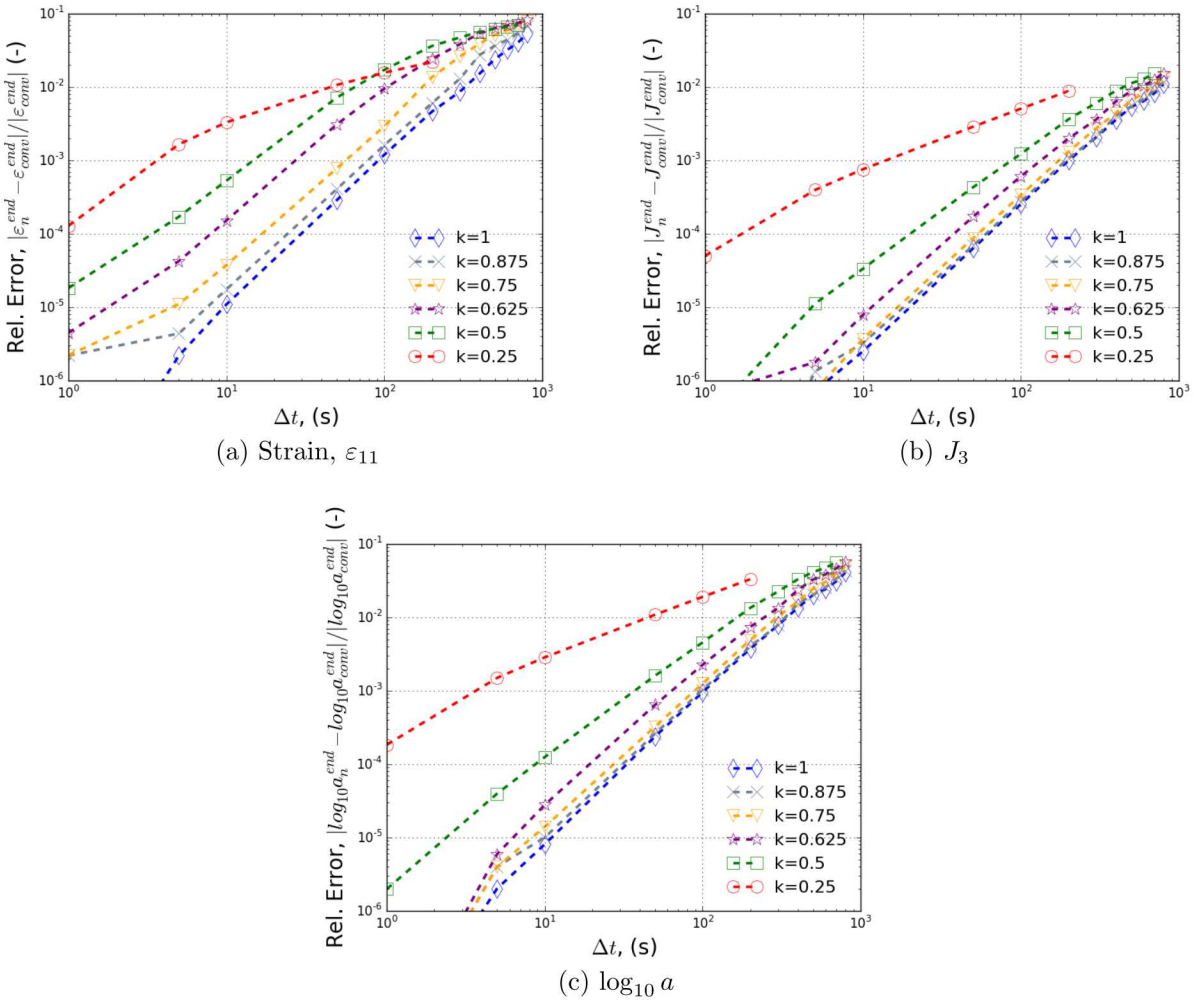

(a) Strain, ε_{11} (b) J_3

(c) $\log_{10} a$

Figure 2: Relative error convergence of (a) strain, (b) J_3, and (c) $\log_{10} a$ through no-load cooling paths with different fixed timesteps. Simulations with $\Delta t = 0.5$s (for each k value) are taken to be the "converged" solutions for purposes of calculating error.

As is expected, it is clear from all three results that error does decrease with timestep size. Additionally, from the $k = 1$ results, the current integration routine recovers the quadratic rate of convergence expected for such a method. By comparing Fig. 2b with Figs. 2a and 2c it may be seen that the hereditary integral value, J_3, exhibits generally lower error for a given

[4]Given the pure thermal loading, a uniform volumetric strain is produced. For convenience, ε_{11} is chosen as a measure of the strain although any of the three normal strains would be equivalent.

timestep than the other quantities. As J_3 is the quantity actually being integrated, such an observation makes sense. With respect to the impact of k, it may also be observed that error increases with increasing non-linearity (decreasing k). This issues seems more pronounced with the strain value. Furthermore, while higher k values keep the approximately quadratic rate of convergence, the $k = 0.25$ responses are clearly closer to linear. Thus, as non-linear temperature profiles are introduced higher error is introduced with this numerical scheme.

For comparison, Fig. 3 presents the convergence results for $k = 1$ (Fig. 3a) and $k = 0.5$ (Fig. 3b) for two different methods – the existing midstep and implicit backward. Note, two results are shown for the existing scheme. Specifically, the finite element results are presented (denoted by an "(N)") alongside a separate implementation "(A)" referred to as analytic for sake of convenience. The "analytic" scheme is a special, reduced form for this load-path implemented in a stand-alone fashion to enable broader consideration of the performance. While minor differences may be observed associated with small difference in implementation (*e.g.* no global solve), clear agreement is noted between the two schemes enabling further study. A similar "analytic" implementation of the backward Euler method (denoted "Imp. $\beta = 1$") is also presented. It recovers the expected linear convergence rate. While the existing midstep scheme does show lower error and a higher convergence rate in both cases, it may be noted that the quadratic convergence in the $k = 1$ case is not preserved with $k = 0.5$ for the midstep scheme. The implicit approach, on the other hand, has a slightly higher overall error but the linear convergence is maintained in both cases. As such, while it has higher error the implicit scheme exhibits less sensitivity to non-linear temperature profiles than the existing midstep approach.

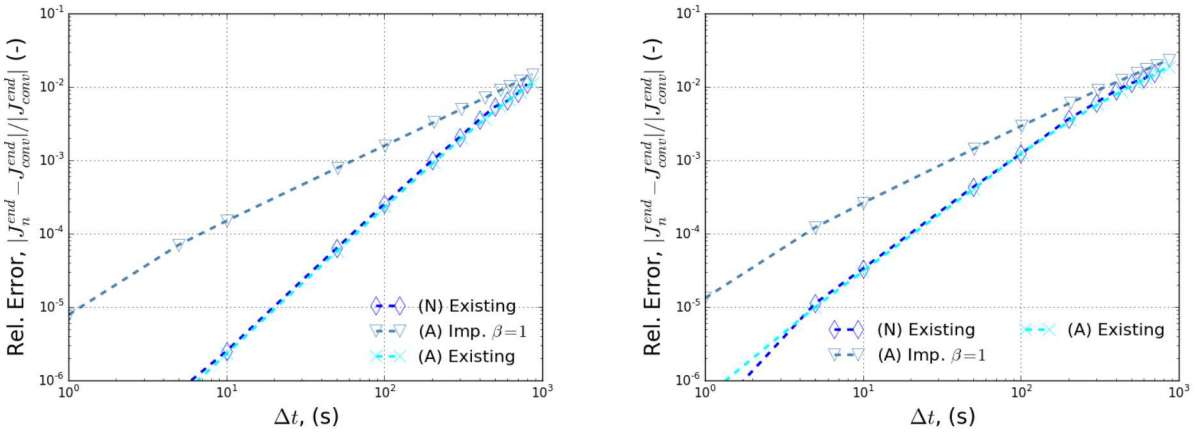

(a) $k = 1$ (b) $k = 0.5$

Figure 3: Relative error convergence of different numerical methods with (a) k=1 and (b) $k = 0.5$. "Existing" refers to the current midstep method with (N) denoting a numerical result from Sierra/SolidMechanics while (A) is for the analytic implementation. The implicit, backward Euler scheme results are also presented and denoted "Imp. $\beta = 1$".

4.2 Creep

Creep tests in which a constant stress is applied and held at a fixed (or variable) temperature for extended duration are a common way of characterizing the viscous responses of viscoelastic materials (*e.g.* [6, 3]). As such, the numerical convergence of the response through such loadings is considered here. A representative schematic of the considered stress-temperature path is shown in Fig. 4. While 3-point bend tests are commonly used for such tests (*i.e.* [3]), here an uniaxial tensile loading is investigated to remove any possible structural effects.

In the considered path, $T\left(t=0\right) = T_{\text{ref}} + 50 = 510°\text{C}$ and cooled at 2°C/min to the creep temperature, T_{creep}, which is $T_{\text{creep}} = T_{\text{ref}} - 50 = 410°\text{C}$ in Fig. 4. The considered tensile load (50 MPa in Fig. 4) is then applied in 5s and the material is then held for a creep time of two hours (120 minutes). Note, some of the loading parameters (*i.e.* cooling rate, loading time, hold time, load values) come from the discussion of Jamison *et al.* [21] in their efforts to model the creep response of a glass-ceramic. For the following comparisons, the "creep-strain", ε^{c}, which is the strain generated in the direction of loading after the load is applied at temperature is used as the metric of interest. In Fig. 4 the "zero" creep time t_{creep} is indicated such that $\varepsilon^{\text{c}}\left(t_{\text{creep}}\right) = \varepsilon\left(t_{\text{creep}}\right) - \varepsilon\left(0\right)$.

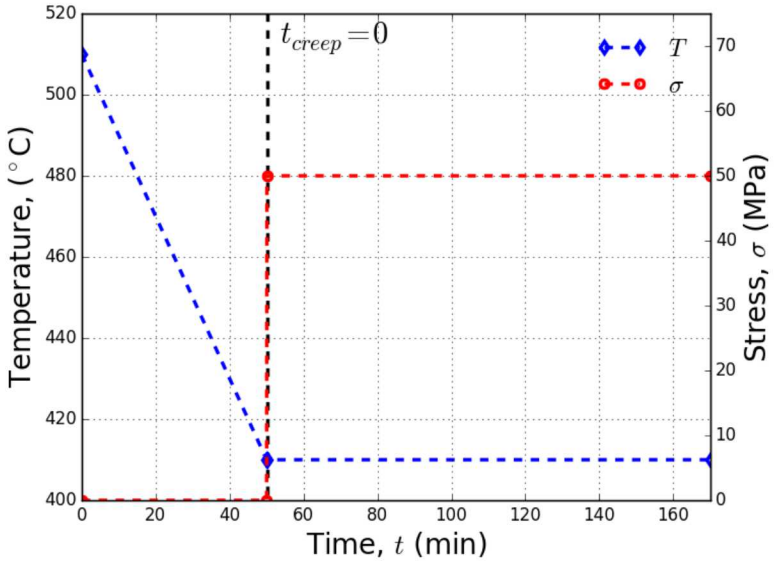

Figure 4: Illustration of creep loading history considered for current studies.

The numerical convergence behavior for different applied loads and creep temperatures is shown below in Fig. 5. Note while different timesteps are used during the creep stage, fixed time increments of $\Delta t_{\text{cool}} = 5\text{s}$ and $\Delta t_{\text{load}} = 0.25\text{s}$ are used during cooling and loading, respectively. To investigate the response, creep temperatures of 360, 385, 410, and 435°C (which correspond to $T_{\text{creep}} = T_{\text{ref}} - 100,\ 75,\ 50$, and 25°C, respectively) and loads of 30, 50, 70, and 90 MPa were considered. Figures 5a and 5b show the influence of temperature and the lowest (30 MPa) and highest (90 MPa) loads while Figs. 5c and 5d consider the coolest

and hottest temperatures at different loads. In the results of Fig. 5, a minimum relative error of 1×10^{-12} was considered.

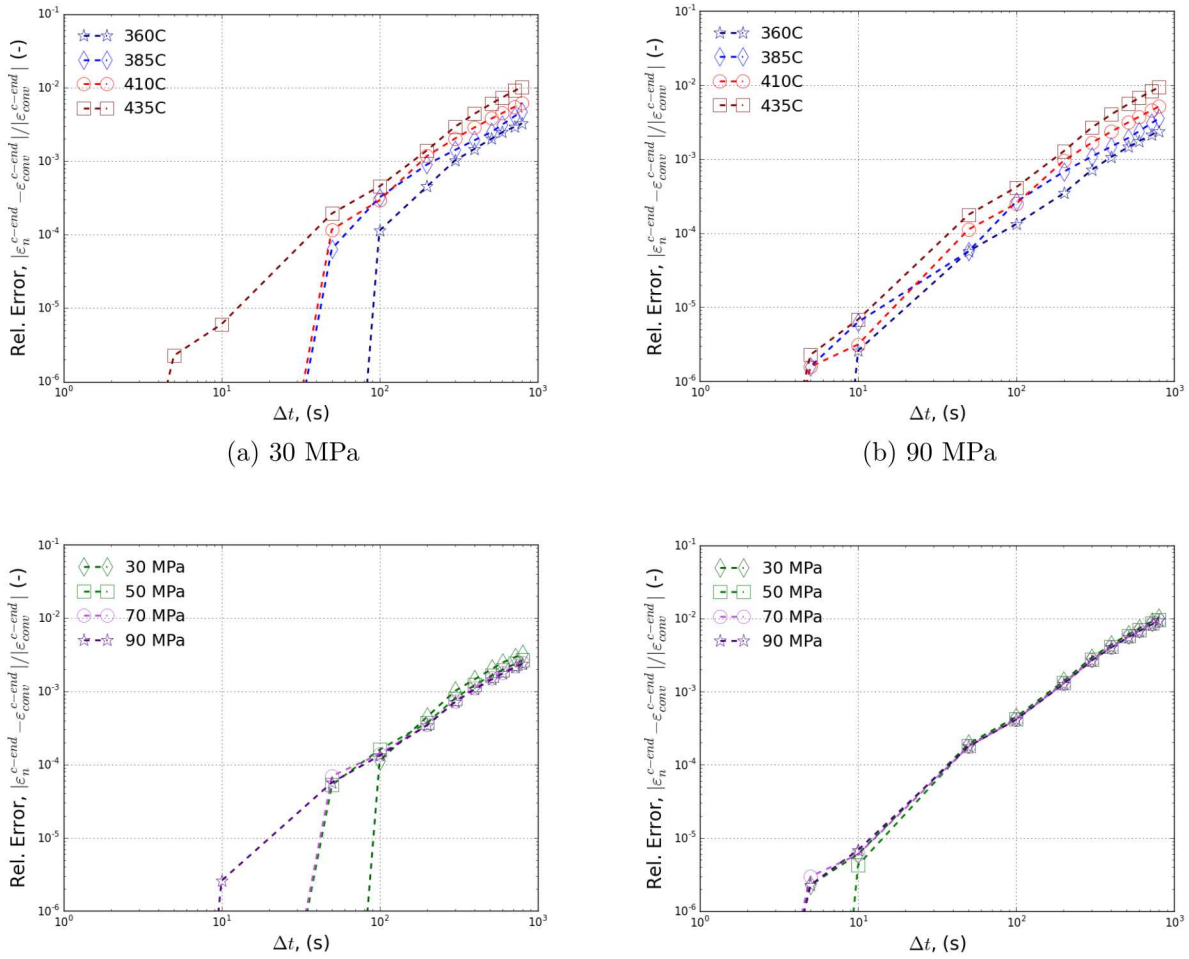

(a) 30 MPa

(b) 90 MPa

(c) $T_{\text{creep}} = 360°\text{C}$

(d) $T_{\text{creep}} = 435°\text{C}$

Figure 5: Relative error convergence of creep strain at various temperatures and loads: different creep temperatures with and applied load of (a) 30 MPa and (b) 90 MPa or various loads at $T_{\text{creep}} =$ (c) 360°C and (d) 435°C. Simulations with $\Delta t = 0.5$s (for each k value) are taken to be the "converged" solutions for purposes of calculating error.

By comparing the results in Fig. 5, the applied stress (at least in the domains considered) seems to have a minor impact on the error. In fact, at the highest temperature considered ($T_{\text{creep}} = 435°\text{C}$) the various curves lie nearly on top of each other. With respect to temperature, however, Figs. 5a and 5b indicate that higher creep temperatures produce larger overall integration errors. In all cases, however, similar slopes and convergence rates may be observed.

4.3 Cooling under Load

In the previous examples, mechanical loading and temperature sweeps were performed separately. To consider the combined effects a modified loading is investigated in which the cooling is performed under load. Specifically, an initially unloaded specimen at $T\,(t=0) = T_{\text{ref}} + 50°\text{C}$ is subjected to a hydrostatic mechanical load p in which $\sigma_{ij} = p\delta_{ij}$ is applied over 10s and then cooled through the various profiles in Fig. 1 with the load held constant. As $C_3 = 0$ there is no asymmetry in the tension-compression response so the loading is tensile for convenience. Additionally, a hydrostatic loading is considered as the J_1 and J_3 hereditary integrals have a common dependence on the volumetric spectra, f_v, and the interaction may be assessed. Furthermore, such a selection means that the deviatoric spectra should have no impact. This loading is schematically illustrated in Fig. 6 for the case of $k = 1$.

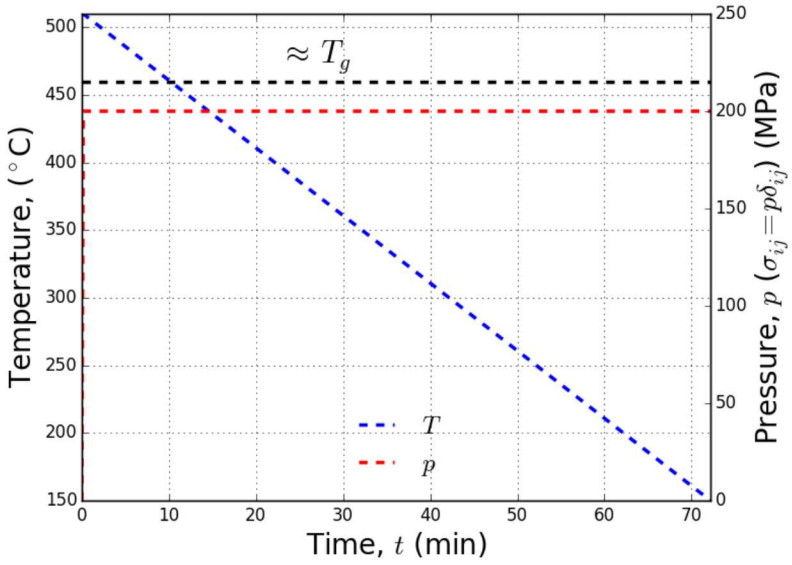

Figure 6: Illustration of cooling under load loading history considered for current studies.

For such loadings, convergence (in terms of the final strain) of the various simulations with timestep are presented in Fig. 7 for mechanical loads of $p = 50$ MPa (7a) and $p = 200$ MPa (7b). While the results given in Fig. 7 show many similar trends to previous results – *e.g.* higher error with smaller k-values – some characteristics are quite different. For instance, with the $k = 0.625$ and other more non-linear cases a near invariance of the strain to timesteps is noted at larger timesteps. Furthermore, the $k = 0.75$ case seems to experience periods with larger convergence rates than the linear response.

In considering the source of these differences, it is noted that the initial loading temperature is above the nominal glass-transition reference temperature and then cooled through that temperature as indicated by the black line in Fig. 6. With larger timesteps, and especially the case of non-linear temperature profiles, a possible consideration is whether or not there

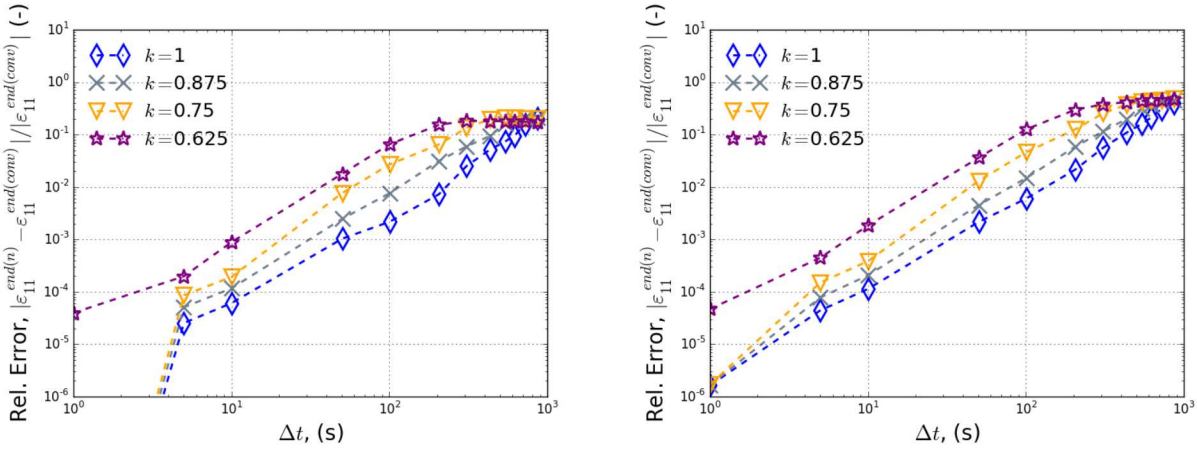

(a) $p = 50$ MPa (b) $p = 200$ MPa

Figure 7: Relative strain error convergence of the cooling under load path with an applied load of (a) $p = 50$ MPa and (b) $p = 200$ MPa. Simulations with $\Delta t = 0.5$s (for each k value) are taken to be the "converged" solutions for purposes of calculating error.

are sufficient timesteps to account for the large change in shift factor associated with glass-transformation. To this end, Fig. 8 presents the number of timesteps for a given temperature profile and timestep size in the rubbery phase (above T_{ref}). This is done by solving Eqn. 30 for the time when $T = T_{\text{ref}}$ and dividing by the corresponding timestep size. As observed in Fig. 8, there are in fact many instances in which there is less than one timestep in the glassy domain.

The impact of the not having sufficient timesteps before the glass-transition may be observed in Fig. 9 in which the strain histories are plotted as a function of time for $k = 1$ (9a) and $k = 0.625$ (9b) with $p = 200$ MPa for all of the different timestep sizes. The assumed converged response (with $\Delta t = 0.5$s) is indicated as a solid black line. Importantly, the lines colored green indicate those with at least one timestep after load is applied in the rubbery phase while red lines are those in which there are no timesteps above T_{ref} after load. From these results, especially Fig. 9b, there is a clear separation of responses between those with and without a timestep in the rubbery domain.

Importantly, in Fig. 9 the final error is not a result of continually compounding errors whose sum increases. Instead, there is a clear and large difference in peak strain immediately after load is applied. Thus, by using too coarse of a timestep issues may arise both regarding final error measures and specific response characteristics like the post-loading strain increase observed in Fig. 9. These observations highlight the impact of careful selection of a integration timestep for a viscoelastic model. The viscous nature of the material phenomenology means there are intrinsic timescale(s) associated with the response and appropriately resolving different characteristics requires considering corresponding numerical integration timesteps. Given the number of viscoelastic spectra and even more numerous characteristic times comprising their Prony series representations arriving at a rule or metric for bounding

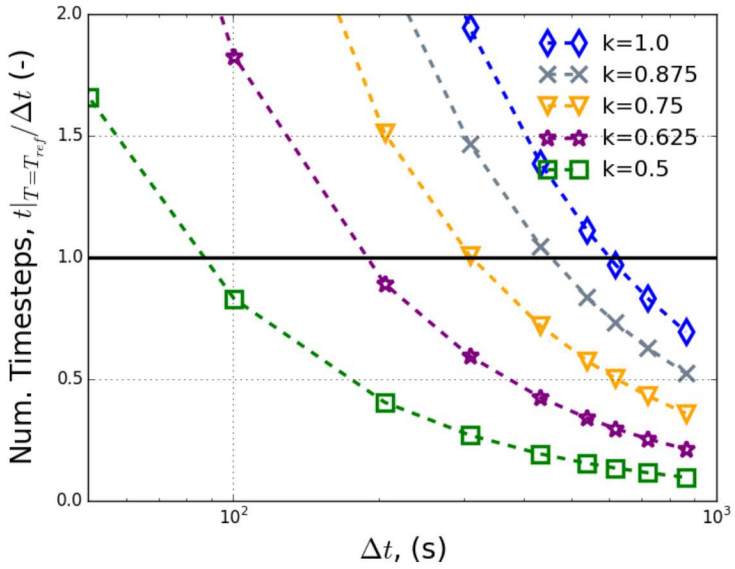

Figure 8: Number of timesteps after load is applied while $T > T_{\text{ref}}$ for the case of cooling under load.

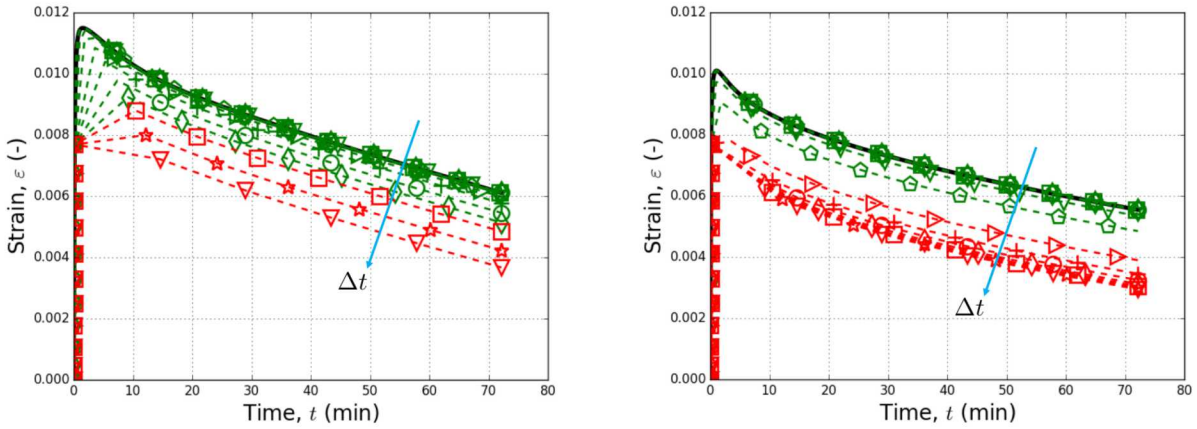

(a) $k = 1$ (b) $k = 0.625$

Figure 9: Strain history through the cooling under load case with $p = 200$ MPa and (a) $k = 1$ and(b) $k = 0.625$ for all the different considered timesteps. The arrows indicate the directions of increasing timestep size which the solid black line indicates the assumed converged response with $\Delta t = 0.5$s. Responses colored green have at least one timestep after loading prior to crossing $T = T_{\text{ref}}$ while the red lines do not have a timestep after loading above $T = T\text{ref}$.

considerations remains a challenge. Adaptive approaches using non-constant timestep sizes may be a path towards addressing this issue. No attempt is made towards either approach

at this time. Instead, this example is used to reinforce the impact of such selections.

5 Conclusion

Non-linear viscoelastic models, including the SPEC formulation, have complex thermomechanical history dependence. Such formulations depend not only on a temperature or single internal state variable history, but also on volumetric and deviatoric loading paths. Therefore, appropriate numerical integration schemes are needed as prerequisites for use in any analysis. The viscous nature of the model further compounds this necessity.

In this work, attempts were made to study the numerical integration scheme of the implementation of the SPEC model. While prior studies have considered simpler viscoelastic forms, the impact of extra non-linearities and complexities in the form of interest have not been assessed. To pursue such an endeavor, a variety of simplified purely thermal loading paths were simulated with different fixed timesteps to assess error and convergence. Results of these efforts demonstrate that even with the additional non-linearities of the SPEC formulation the numerical integration is able to reproduce some of the desired behaviors observed during earlier iterations in the considered loadings.

Generally speaking, the performance of the model was as desired and a quadratic rate of convergence was observed as expected for a midstep integration scheme. Comparison to a backward Euler scheme again demonstrated superior convergence and smaller error for the considered loading cases. However, by considering temperature paths with increasing non-linearity it was observed that error generally increased with the deviation form linearity although the implicit backward Euler convergence rates were less sensitive to this issue.

To assess the behavior of combined thermomechanical loading paths, a variety of creep simulations were performed with different histories. In these cases, the model did generally exhibit desired behaviors for convergence and broadly speaking error seemed to be more sensitive to temperature rather than load. By performing coolings under load, in which the load is applied above the reference glass-transition temperature, it was demonstrated that appropriate selection of the timestep can have a large impact on the predicted responses and corresponding errors if too coarse with respect to material phenomenology. These issues highlight the impact of considering the numerical timestep resolution with desired physical response and load-path as the complex history dependence of the viscoelastic model compounds the impact of numerical approach.

Acknowledgements

The authors would like to thank B. Elisberg for valuable insight during review of this document. Sandia National Laboratories is a multimission laboratory managed and operated by National Technology and Engineering Solutions of Sandia, LLC., a wholly owned subsidiary of Honeywell International, Inc., for the U.S. Department of Energy's National Nuclear Security Administration under contract DE-NA0003525. This paper describes objective technical

results and analysis. Any subjective views or opinions that might be expressed in the paper do not necessarily represent the views of the U.S. Department of Energy or the United States Government.

Bibliography

[1] J. Caruthers, D. Adolf, R. Chambers, P. Shrikhande, A thermodynamically consistent, nonlinear viscoelastic approach for modeling glassy polymers, Polymer 45 (2004) 4577–4597.

[2] O. S. Narayanaswamy, A model of structural relaxation in glass, Journal of the American Ceramic Society 54 (10) (1971) 491–498.

[3] R. Chambers, R. Tandon, M. Stavig, Characterization and calibration of a viscoelastic simplified potential energy clock model for inorganic glasses, Journal of Non-Crystalline Solids 432 (2016) 545–555.

[4] B. D. Coleman, W. Noll, Foundations of linear viscoelasticity, Review of Modern Physics 33 (2) (1961) 239–249.

[5] R. M. Cristensen, Theory of Viscoelasticity, 2nd Edition, Dover Publications, Inc., Mineola, NY, 2003.

[6] D. B. Adolf, R. S. Chambers, M. A. Neidigk, A simplified potential energy clock model for glassy polymers, Polymer 50 (2009) 4257–4269.

[7] R. A. Schapery, On the characterization of nonlinear viscoelastic materials, Polymer Engineering and Science 9 (4) (1969) 295–310.

[8] R. L. Taylor, K. S. Pister, G. L. Goudreau, Thermomechanical analysis of viscoelastic solids, International Journal for Numerical Methods in Engineering 2 (1970) 45–59.

[9] R. S. Chambers, E. B. Becker, Integration error controls for a finite element viscoelastic analysis, Computers & Structures 24 (4) (1986) 537–544.

[10] R. Chambers, Numerical integration of the hereditary integrals in a viscoelastic model for glass, Journal of the American Ceramic Society 75 (8) (1992) 2213–2218.

[11] R. M. Haj-Ali, A. H. Muliana, Numerical finite element formulation of the Schapery non-linear viscoelastic material model, International Journal for Numerical Methods in Engineering 59 (2004) 25–45. doi:10.1002/nme.861.

[12] A. Muliana, K. A. Khan, A time-integration algorithm for thermo-rheologically complex polymers, Computational Materials Science 41 (2008) 576–588.

[13] G. A. Holzapfel, On large strain viscoelasticity: Continuum formulation and finite element applications to elastomeric structures, International Journal for Numerical Methods in Engineering 39 (1996) 3903–3926.

[14] J. Simo, T. Hughes, Computational Inelasticity, Vol. 7 of Interdisciplinary Applied Mathematics, Springer-Verlag, New York, NY, 1998.

[15] D. B. Adolf, R. S. Chambers, J. M. Caruthers, Extensive validation of a thermodynamically consistent, nonlinear viscoelastic model for glassy polymers, Polymer 45 (2004) 4599–4621.

[16] D. B. Adolf, R. S. Chambers, J. Flemming, J. Budzien, J. McCoy, Potential energy clock model: Justification and challenging predictions, Journal of Rheology 51 (2007) 517–540.

[17] M. L. Williams, R. F. Landel, J. D. Ferry, The temperature dependence of relaxation mechanisms in amorphous polymers and other glass-forming liquids, Journal of the American Chemical Society 77 (1955) 3701–3707.

[18] LAMÉ Team, Library of advanced materials for engineering (LAMÉ) 4.52, Tech. Rep. SAND2019-3058, Sandia National Laboratories, Albuquerque, NM 87185 and Livermore, California 94550 (March 2019).

[19] U. M. Ascher, C. Greif, A first course in numerical methods, Computational Science & Engineering, SIAM, Philadelphia, PA, 2011.

[20] SIERRA Solid Mechanics Team, Sierra/SolidMechanics 4.50 user's guide, SAND Report 2018-10673, Sandia National Laboratories, Albuquerque, NM 87185 and Livermore, CA 94550 (2018).

[21] R. D. Jamison, A. M. Grillet, M. E. Stavig, K. Strong, S. Dai, Assessing the validity of the simplified potential energy clock model for modeling glass-ceramics, Tech. Rep. SAND2017-10893, Sandia National Laboratories, Albuquerque, NM 87185 and Livermore, California 94550 (October 2017).

Internal Distribution:

MS-0346 J. Bishop
MS-0346 B. Elisberg
MS-0346 K. Ford
MS-0346 S. Grutzik
MS-0346 B. Owens
MS-0840 H. E. Fang
MS-0840 B. Lester
MS-0840 K. Long
MS-0840 C. Vignes
MS-0889 D. Reedy
MS-9042 S. Nelson
MS-9042 A. Skulborstad
MS-9042 B. Talamini